Formetta, Giuseppe; Capparelli, Giovanna. 2019. **Quantifying the three-dimensional effects of anisotropic soil horizons on hillslope hydrology and stability**

Quantifying the three-dimensional effects of anisotropic soil horizons on hillslope hydrology and stability.

Giuseppe Formetta[1] and Giovanna Capparelli[2]

[1]Centre for Ecology & Hydrology, Crowmarsh Gifford, Wallingford, UK

[2]University of Calabria Dipartimento di Ingegneria Informatica, Modellistica, Elettronica e Sistemistica Ponte Pietro Bucci, Cubo 41/b, 87036 Rende, Italy

Quantifying the three-dimensional effects of anisotropic soil horizons on hillslope hydrology and stability.

Giuseppe Formetta[1] and Giovanna Capparelli[2]

Abstract

Rainfall-induced shallow landslides cause significant damage involving loss of life and property. Many hydrological processes such as rainfall infiltration, soil water dynamics, and slope stability are controlled by unsaturated soil properties, such as unsaturated hydraulic conductivity. Natural soils often exhibit a certain degree of anisotropy in hydraulic conductivity due to stratification and compaction mechanisms in soil formation processes.

In this paper we investigate the effect of soil hydraulic conductivity anisotropy (SHCA) on hillslope hydrology and stability using a three-dimensional hydrological model coupled with a probabilistic infinite slope stability model. The model is applied in two independent case studies. The first aims to quantify the combined effect of different anisotropy ratios (lateral/normal saturated hydraulic conductivity) and hillslope morphologies (convex, concave, and planar) on slope stability. Anisotropy ratios are assumed in this case higher than one (1, 2, 10). Results show that increasing the anisotropy ratio (from 1 to 10) anticipates the failure time (from 12 to 9 hours after the start of rainfall) and that in concave morphologies the unstable area tends to be wider than planar and convex. The second application aims to simulate the

soil moisture dynamic and the probability of failure at different depths (100, 500, and 900 mm) of a stratified volcanic soil, making leverage on the model flexibility to accommodate SHCA. No assumptions are made on the anisotropy ratio in this case study. Our results, based on model parameter calibration and verification against in-situ soil moisture measurements during the year 2009, showed good model performance in simulating the soil moisture dynamic (Kling-Gupta Efficiency higher than 0.78) and confirmed no failure for the simulated year. The promising results support the aspiration that the physically based hydrological model can complement and improve the current predictions of landslide early warning systems.

Introduction

Landslides are one of the most dangerous natural hazards, causing thousands of deaths and billions of dollars in damage worldwide each year (Hong et al., 2006, International Federation of Red Cross and Red Crescent Societies, 2003). Shallow landslides, in particular, are very catastrophic due to their high speed of development and intensity. They often mobilize into rapidly moving debris or earth flows (Iverson et al., 1997), representing a dangerous hazard to human life and social and economic activities (e.g., Sidle and Ochiai, 2006; Keefer and Larsen, 2007).

In order to avoid such disasters, accurate prediction of landslide triggering time and location is crucial. In recent years several approaches have been developed to predict landslide-prone areas. Many studies provide an accurate overview and description of these methods (Carrara et al., 1999; Guzzetti et al., 1999; Corominas et al., 2014).

Physically based deterministic models simulate the triggering causes of landslides as interaction between hillslope hydrology, geology, geomorphology, and slope stability. For this reason they are powerful in physically understanding the triggering process and in predicting its timing and location. They are usually based on digital elevation models of the terrain and require hydro-geomorphological input data (such as rainfall, slope, aspect, terrain curvature maps) and geological-geotechnical input data (such as soil hydraulic conductivity, friction angle, soil and root cohesion). Physically based deterministic models usually provide a safety factors (FS, ratio of stabilizing and destabilizing forces) for each pixel or its probability of failure (probability that FS<1 for that location). They have varying degrees of complexity according to the hypothesis on the hydrological and slope stability model they use. The hydrological model component is usually based on the steady state hypothesis (Montgomery and Dietrich, 1994; Pack et al., 1998; Park et al., 2013); quasi-steady state hypothesis (Wu and Sidle, 1995; Barling et al., 1994; Borga et al., 2002; Lanni et al., 2013); and transient infiltration models based on approximations of the Richards equation (Baum et al., 2010; Capparelli and Versace 2011; Lepore et al. 2013; Tsai and Yang, 2006; Mirus et al., 2007; Simoni et al., 2008; An et al., 2016). Baum et al. (2010) use a solution of the one-dimensional Richards equation with the Gardner (1958) soil-water retention curve. Models such as An et al. (2016) mostly use an approximation of the 3D subsurface, solving the vertical flow implicitly and the horizontal flow explicitly. This is based on the hypothesis that horizontal flow is far slower than vertical flow. Applications of physically based models for slope cross-sections take into account different material strata (or single strata

discretized into layers) and variations in saturated hydraulic conductivity. The latter, in the absence of borehole data, is usually assumed to increase as depth increases. Other physically based approaches to modeling slope stability include analysis of continua (e.g. the Fast Lagrangian Analysis of Continua, Itasca, 2000) and two-phase flows (e.g. Iverson et al., 2000). Physically based geo-mechanical models are valid tools for assessing the impact of unsaturated hydraulic properties on slope stability (e.g. Mirus et al., 2016; Chen et al., 2017; Thomas et al., 2018). Although anisotropy in soil hydraulic conductivity, together with the slope gradient, is known to be responsible for the subsurface lateral redistribution of soil moisture (Lu and Godt, 2013), its impact on slope instability has not been well established. It is generally accepted that a soil can exhibit a form of apparent anisotropy due to the combined effect of multiple pedogenic horizons with decreasing hydraulic conductivities with depth. This explains, for example, lateral spreading during ponded infiltration experiments (e.g. Nimmo et al., 2009; Mirus et al., 2009).

Most of the studies that aim to understand to role of rainfall infiltration in unsaturated flow on slope stability (e.g. Ng and Shi 1998; Kasim et al. 1998; Affuso et al. 2000; Lu and Godt, 2008) have been carried out considering soil hydraulic conductivity as isotropic. Few studies have pointed out the influence of hydraulic conductivity anisotropy on pore-water pressure. Mirus (2015) assessed the impacts of explicitly accounting for soil layers versus effective anisotropy using a coupled model of the 3D Richards equation and 2D overland flow. He found that the anisotropy ratio could only partially explain the complex variably-saturated hydrologic response dynamics in layered hillslope soils. Differently from Mirus (2015), in the present study we seek to

extend this approach by using distinct soil layers and eventual anisotropy in each individual soil layer. Dong and Hsu (2011) showed that neglecting the hydraulic conductivity anisotropy leads to an overestimation of the safety factor. Yeh et al. (2015) used a two-dimensional infiltration model to simulate the instability condition of a simplified planar hillslope with a slope angle of 30 degrees. They found that, in the anisotropic case, slope instability occurs earlier than the case of isotropic soil hydraulic conductivity. Lepore et al. (2013) investigated the effect of soil hydraulic conductivity anisotropy using a physically based model that involved: i) numerical approximation of the one-dimensional Richards equation (Hillel, 1980) and ii) a lateral redistribution of subsurface and surface moisture among the cells along the direction of steepest descent with a rate depending on the unsaturated hydraulic conductivity of the receiving cell.

In this paper we present and test GEOtop-FS 2.0, an open source 3-D slope stability model preliminarily applied in Formetta et al. (2016) and Formetta et al (2014). It is based on the fully three-dimensional hydrological model GEOtop 2.0 (Endrizzi et al., 2015; Rigon et al., 2006; Bertoldi et al., 2006), it implements the suction stress theory (Lu and Likos, 2006) for the computation of the effective stress under variably saturated conditions, and uses a probabilistic framework for the calculation of (in)-stability conditions.

It is based on the infinite-slope model widely used for modeling the stability of translational landslides (Dietrich et al., 1995; Baum et al., 2010). The infinite slope model simulates failure at a given depth, assumes contrast between the soil properties of a substrate and an overlying material and hypothesizes a failure surface parallel to the slope. Among other methods for performing

slope stability analysis, limit-equilibrium methods (e.g. Fellenius, 1936; Bishop, 1955; Morgenstern and Price, 1965; Janbu, 1973) and their combination with finite element methods (e.g. Matsui and San, 1992; Smith and Griffiths, 2004) are those most widely used. The former are based on a discretization of the hypothesized failure slope into vertical slices and compute the FS using the principles of force and/or moment equilibrium; the latter use numerical algorithms for shear strength reduction analysis in the context of finite element methods. Finally, Lu et al. (2012) proposed the local factor of safety method (LFS), which provides a scalar field of FS, based on the concept of Coulomb stress and the shift of stress paths toward the failure state in slopes under variably saturated infiltration. Unlike the previous approach, the novel method does not hypothesize any potential failure surface.

Recently many efforts have been devoted to calibrating and validating physically based models for landslide prediction. The former aims to select an optimal model parameter set to minimize the difference between observations (such as soil moisture/pressure head measurements, landslide/no landslide areas) and simulation results (e.g. Gioia et al., 2016; Formetta et al., 2016; Zieher et al., 2017). The latter includes different methodology to assess the ability of the model to reproduce actual landslides (Frattini et al., 2010; Guzzetti et al., 2006; Formetta et al., 2016; Mergili et al., 2018).

The paper is organized in four sections. Each model component is presented in Section 2 as well as the differences with respect to the previous GEOtop-FS (Simoni et al., 2008) version. We present and discuss two model applications in Section 3. The first extends the case study presented in

Formetta et al. (2016). The second involves a new case study in the Tuostolo river basin (Sarno, Italy), where rainfall and soil moisture measurements at different depths were recorded for one year at hourly time steps.

Formetta et al. (2016) sought to ascertain the effect of different real slope morphologies (concave, convex, and planar) on slope hydrology and stability under the hypothesis of uniform rainfall in time and isotropic soil. Moreover, the model results were not verified against measured data (such as soil moisture or soil pressure) due to the lack of monitoring instruments in the study area. In this paper we removed the assumption of isotropic soil in order to quantify the effects of soil hydraulic conductivity anisotropy on hillslope hydrology and stability. Results are provided for different geomorphologies (concave, convex, and planar) and for different anisotropy ratios $r = K_h / K_v$ (ratio between lateral and slope normal saturated hydraulic conductivities) in terms of pressure head, water content, suction stress, and probability of failure for different soil depths.

The second case study is located in the Sarno area (Campania, Italy), where rainfall-induced shallow landslides sadly constitute one of the most frequently occurring natural hazards. The complex stratigraphic sequences of the soil and the high variability of the hydraulic/mechanical properties (Di Crescenzo and Santo, 2005; Orsi et al., 2004; Picarelli et al., 2006) are the main factors controlling soil instability in the area. Various approaches have been applied to understand and eventually predict the failure mechanism and propagation such as: i) unsteady non-uniform flow modeling (e.g. Revellino et al., 2004), smoothed-particle hydrodynamics (SPH) modeling; ii) rainfall threshold definition for landslide triggering (e.g. Rossi and Chirico, 1998; De Vita et al.

2013); iii) combining physically based hydrologic modeling and hydrologic monitoring (De Vita et al., 2013; Napolitano et al., 2016; Fusco et al., 2017); and iv) coupling one/two dimensional resolution of the Richards equations with a slope stability model (e.g. Cascini et al., 2011; Capparelli and Versace, 2014; Damiano et al., 2017). The latter approaches usually investigated the event by using event-based models which: a) usually neglect evapotranspiration processes and b) are strongly dependent on the soils' initial conditions. Napolitano et al. (2016) presented a two-dimensional continuous simulation for modeling soil suction, neglecting the effect of anisotropic hydraulic conductivity in the soil layers.

Previous studies in the Sarno area have observed the presence of hydraulic heterogeneity and anisotropy in the topsoil and in the bedrock through measurement campaigns (e.g. De Vita and Piscopo, 2002; Arnalds et al., 2007; Vingiani et al., 2015). Most of them obtained an anisotropy ratio higher than one, which has been already used in some simplified physically based modeling framework applied in the area (e.g. Frattini et al., 2004).

In this paper, differently from other applications, we use a continuous modeling simulation approach which involves the resolution of the three-dimensional Richards equations, including the effects of anisotropic hydraulic conductivity, which can be specified for individual soil units, not the soil as a whole. The application is made of two steps. The first step involves estimating hillslope hydrological properties by automatic calibration of the model parameters, using on site measurements of soil moisture in one location at three different depths (100, 500, and 900 mm). In the second step, using the optimal parameter set previously computed, we estimated the evolution in

time of failure probability at different depths in the entire simulation period.

2. Methodology

2.1 Modeling framework

The hillslope hydrology and stability analysis carried out in this paper are based on the GEOtop-FS 2.0 modeling framework presented in Figure 1. The framework integrates: i) the open source three-dimensional fully distributed hydrological model GEOtop 2.0 (Endrizzi et al., 2015), ii) a space and time varying hillslope stability component based on the infinite slope model, iii) an open source Geographic Information System (uDig-JGrass GIS) for the creation of the model input maps and the visualization of the model output, and iii) a set of automatic model parameter calibration algorithms to estimate the optimal parameter set. OMS capabilities have been intensively exploited and explained in detail in many hydrological applications such as modeling river flows and snow-melting evolution (Formetta et al., 2011; Formetta et al., 2014A; Formetta et al., 2014B; Abera et al., 2017A; Abera et al., 2017B), quantifying energy balance (Formetta et al., 2013; Formetta et al., 2016), framework invasiveness on specific hydrological models (Lloyd et al., 2011), and soil moisture and soil temperature modeling (Formetta et al., 2016). In this study OMS was used for two tasks: i) to connect the GIS udig-JGrass and the model GEOtop in order to create the input maps (such as slope, curvature, aspect) and visualize the output maps (such as pore water pressure and failure probability maps); and ii) to connect the OMS-Luca (Hay et al., 2006; Formetta et al., 2016) calibration algorithm and GEOtop model to calibrate the van Genuchten-Mualem parameters for each soil layer using the

measured soil moisture data available in one location at different depths.

The GEOtop 2.0 hydrological model (Rigon et al., 2006; Endrizzi et al., 2014) is a high-resolution distributed water and energy budget model for small catchments and complex terrain. It models surface and subsurface flows of variably saturated soil, snow cover dynamics, soil freezing, and terrain effects. The model is based on a three-dimensional finite volume approach and couples heat and the water flow equations using the time-lagged approach proposed in Panday and Huyakorn (2004). The three-dimensional Richards equations (Richards, 1931) are solved to calculate unsaturated and saturated flows: the former uses the van Genuchten (1980) soil water retention curve, the latter used the linear concept of specific storativity. Overland flow is based on the extension of Darcy's law to surface flow as proposed in Gottardi and Venutelli (1993), and channel routing is modeled by the shallow water equation neglecting the inertia. The GEOtop 2.0 is connected with the uDig-JGrass GIS for the input-output visualization process (Formetta et al., 2016) and to the hillslope-stability model for the computation of the safety factor (see Formetta et al., 2016 for details). It involves the computation of soil moisture, soil suction, and probability of failure using the infinite slope model for each cell of the computational domain (and assuming in turn the depth of each layer as potential failure surface). The model uses the suction stress theory that allows the computation of the effective stress ensuring a mathematically consistent description of transition between saturated-unsaturated states. The potential unstable areas are detected using the infinite slope approximation for the computation of the factor of safety, defined as the ratio between stabilizing and destabilizing forces (Taylor, 1948). Finally for each layer of soil

of the computation domain the model provides the failure probability, which is computed using the First Order Second Moment method (Dai and Lee, 2002; Baecher and Christian, 2005, Formetta et al., 2016). A detailed description of the geo-mechanical model component is given in Appendix 1.

The model inputs are: i) meteorological data (rainfall, air temperature, solar radiation, air humidity), ii) raster maps such as digital elevation model, river network, soil types, land cover), iii) physical parameters such as soil water retention and hydraulic conductivity functions for each layer of soil, soil cohesion and friction angle; iv) simulation parameters such as start date, end date, time step; and v) numerical parameters such as tolerances, maximum iteration number. The model outputs are maps of soil moisture, pressure head, suction stress, and failure probability for each soil layer of the computation domain.

2.2 Differences between GEOtop-FS and GEOtop-FS 2.0

The physically based model GEOtop-FS 2.0 differs from GEOtop-FS (Simoni et al., 2008) both in the hydrological and for the slope stability component. From the hydrological point of view, the main differences and improvements are due to the use of the GEOtop 2.0 model (Endrizzi et al., 2014) and consist in: 1) the use of a fully three-dimensional description of the Richards equation, whereas in Simoni et al. (2008) the equation was only solved in the vertical direction and the lateral flow was parameterized; 2) the possible use of distributed meteorological forcing data (such as rainfall, air temperature, humidity) based on the approach of Liston et al. (2006); 3) numerical improvements to the energy budget model, which enable direct coupling of

the surface energy balance with the soil heat equation; 4) the channel routing and the overland flow, described by the shallow-water equation instead of using the geomorphological unit hydrograph theory. The hillslope-stability analysis benefits from the improvements implemented in GEOtop-2.0 and includes a more accurate and physically based representation of hillslope hydrology. Advances have been made from the model implementation perspective (Formetta et al., 2016), which include the use of GIS to manage the input-output raster maps and, more importantly, the use of automatic calibration algorithms to estimate the optimal parameter set using measured data such as soil moisture or pressure head.

3. Study areas and model applications

3.1 Application 1

The first application aims to understand the effect of various real slope morphologies (concave, convex, and planar) on slope hydrology and stability under the hypothesis of anisotropic soil hydraulic conductivity. The model setup and study area are presented in details in Formetta et al. (2016). The morphologies are extracted from 10 m digital elevation model data (Esri asc format) made available by the Friuli regional authority, in the eastern Italian Alps (Figure 2), using the uDig spatial toolbox (Abera et al., 2014). Each of the basins is approximately 10 km^2 in size. The study area is highly eroded mainly because of a large landslide that occurred in 1817 (Castiglioni, 1962) in response to a heavy rainfall event. The concavity/planarity/convexity of a site is computed using the second derivative in space of the elevation $\nabla^2 z$. A cell is planar if $\nabla^2 z = 0$, convex if $\nabla^2 z < 0$, or concave if $\nabla^2 z > 0$. The model

GEOtop-FS 2.0 is applied over the three morphologies assuming a constant soil thickness of 1.5 m over the entire area discretized in 30 layers. The rainfall forcing data were assumed to be similar to the events occurring during and after late summer storms, which often generate shallow landslides in the area. We used a synthetic hyetograph of 12 h rainfall with an intensity of 18 mm/h, and we ran the simulations for 48 h (see also Formetta et al., 2016). The initial conditions were set by fixing the water table height at 2.0 m depth; the model assumes a hydrostatic profile of initial water pressure for the unsaturated zone. The soil is homogeneous silty sand. Laboratory tests on specimens sampled at the experimental site were used to determine the soil water retention curve and hydraulic conductivity function parameters (see Table 1). For each morphology direct shear tests under field conditions were performed at one-meter depth to determine the soil friction angle $\phi' = 34^\circ$ and the soil cohesion 5 kPa. Unlike Formetta et al. (2016) who assume isotropic hydraulic conductivity (r=1), we investigated the impact of three different hydraulic conductivity anisotropy ratios (r=1,2,10) on hillslope hydrology and the corresponding influence on slope stability.

3.2 Application 2

The study area is located in the upper Sarno basin (Campania, Southern Italy), near to the slope side where complex slope failures (initiated as soil slips and transitioned into debris flow) occurred on 5 May 1998, destroying many villages (Del Prete et al., 1998; Esposito et al., 2004).

Several upland areas in Campania are covered by ash-fall pyroclastic

deposits in primary deposition, generally in unsaturated conditions. They are periodically subjected to rainfall-induced landslides that may evolve into catastrophic flowslides. Typically, the maximum overall thickness of such deposits is up to a few meters, but triggered landslides can progressively incorporate the material found along their path, reaching a size of some tens of thousands of cubic meters. Under the top active soil is a pyroclastic cover, i.e. a sequence of ash (silty-sand) layers and pumiceous (gravelly-sand) layers (Capparelli and Versace, 2011), lying on intensely fractured limestone (bedrock). In the stratigraphy we mainly focus on the ash layers that are considered to be responsible for the evolution into flowslides (Olivares and Damiano, 2007).

The availability of experimental observations from monitoring, from in situ and laboratory investigations allows appropriate calibration and validation of the physically-based hydrological model, which can lead to a better understanding of the dynamics causing such instability. A measurement station was instrumented with soil moisture (TDR), rainfall and air temperature measurement devices in order to monitor the hydrologic response of the slope to rainwater infiltration. An automatic system was installed for real-time data acquisition and transmission. Continuous measurements of rainfall and soil moisture at different depth (100, 500, and 900 mm) were collected for the year 2009 and used for model parameter calibration/validation. Figure 3 shows some details describing the area involved in the monitoring process. In particular, Figure 3a shows the landslide shapes and the locations of affected urban areas and Figure 3b details where the monitoring station was located.

Following Capparelli and Versace (2011) the soil was discretized into five

layers from top to bottom. In sequence we have layers of: 1) topsoil (600 mm); 2) coarse pumice (350 mm); paleosoil (type 1, 500 mm); 3) finer pumices (350 mm); 4) paleosoil (type 2, 450 mm); and 5) dark-red clayey ash in contact with the bedrock (200 mm). We assumed constant meteorological input data over the whole basin equal to the hourly-recorded rainfall and air temperature at the monitoring station (Figure 3b). They are the minimum meteorological input data required to solve the coupled energy-water balance.

The model assumes different parameters for each layer in terms of soil water retention and soil hydraulic conductivity functions. The simulation period (year 2009) was split up into a calibration period (from January to March) and a validation period (from March to December). The measured soil moisture time series available at three different depths (100, 500, and 900 mm) was used to: i) calibrate the model parameters (normal and lateral saturated hydraulic conductivity and van Genuchten-Mualem parameters for each soil layer, see Table 2 parameters in bold) and ii) validate the model output.

The soil strength parameters were obtained from laboratory tests on specimens sampled at the experimental site. Specifically, direct shear tests under field conditions were used to determine the shear strength parameters of the soils for each soil layer (see Table 2). Although we assumed that their values were constant for each pixel of the river basin, we attempted to model their uncertainty by using the probabilistic FOSM method. To calibrate the model parameters and quantify the model performance we used the Kling-Gupta efficiency as objective function (KGE, Gupta et al., 2009). It varies between 1 and minus infinity, where 1 indicates a perfect fit between simulated and observed data. The calibration phase carried out for the van

Genuchten and hydraulic conductivity parameters involves definition of the ranges in which they can vary. For the hydraulic conductivities the model does not assume any a priori hypothesis on isotropic or anisotropic conditions but automatically makes them vary in the pre-defined range. This flexibility also allows the possible case of isotropic hydraulic conductivity conditions to be managed.

4. Results and discussion

4.1 Application 1

The model GEOtop-FS 2.0 provides maps of pressure head and failure probability for each layer of the computational domain. Because of the lack of in situ measurement stations we did not use observed pressure head time-series to evaluate the simulated soil moisture dynamics. Results are presented in terms of failure probability for different layers (300, 600, 900, 1200, and 1500 mm), for four different time steps (6, 9, 12, and 24 hours after the simulation start), and for different morphologies (concave, convex, and planar). To assess the impact of morphology and the soil anisotropy ratio on slope hydrology and stability, we present the results as a function of the slope angle. Results are presented for different soil anisotropy ratios, r=1, r=2, and r=10 (Figures 5-7). Figures A1, A2, and A3 (Appendix 1) present the same results in terms of pressure head.

Figure 5 (r=1) reproduces the results presented in Formetta et al. (2016): the instability occurred 24 hours after the event at 1200 mm depth. The concave morphologies (blue points) present the higher probability of failure and tend to be unstable earlier compared to the other morphologies (convex in red and

planar in black), for the same slope angle. Figures 6 and 7 refer to a small (r=2) and a high (r=10) anisotropy ratio, respectively. Hydraulic conductivity anisotropy tends to anticipate the time of failure and to accentuate the differences between the different morphologies. Considering the case r=2 (Figure 6), although instabilities occur at the same time as r=1, the failure probability tends to be higher compared to the case r=1, independently of the morphology, considering the same slope angle. Moreover, compared to the case r=1, the differences between morphology behavior tends to be more evident. Considering the case r=10 (Figure 7), instability occurs 12 hours after the event starts. Also in this case the failure probability tends to be higher compared to cases r=1 and r=2, regardless of the morphology, considering the same slope angle. Finally, while for concave and planar morphologies instability occurs at 1500 mm depth, for concave morphologies it involves a higher portion of the soil column (from 600 to 1500 mm depth).

4.2 Application 2

The model GEOtop-FS 2.0 provides maps and time series of soil moisture dynamic at different depths of the computational domain. In this application we used the soil moisture time series measured at 100, 500, and 900 mm depth to calibrate and validate the model results for the simulation period 2009. Table 2 presents the optimal model parameter set for the calibration period. Figure 8 shows the model results for the three depths: the model simulation is presented in black and the measured data in gray. The optimal model parameters have the same order of magnitude of results presented in other studies in the same area (Capparelli and Versace, 2011; Capparelli and

Versace, 2014; Damiano et al., 2017). A comparison of our results against measured soil parameters for the same area and similar stratigraphy provided in Fusco et al. (2017) shows that saturated hydraulic conductivities are mostly of the same order of magnitude while differences have been found in van Genuchten's parameters especially for the pumices. Finally, although the values used for the bedrock cohesion and friction angle are slightly lower than other studies, we accounted for the uncertainty in their values by using the first order second moment method.

The normal and lateral soil hydraulic conductivities were calibrated independently in order to accommodate possible anisotropy ratios other than 1 in each soil layer. Our results show that for the optimal parameter set the anisotropy ratio varies between around 1 (for the topsoil) and around 3.0 (for the paleosoil type 2). The model is able to simulate the measured soil moisture temporal patterns at different soil depths both in terms of variation in time and in terms of peak magnitude, which is essential for the triggering of shallow landslides. The KGE values computed for simulated and measured soil moisture for the layers at 100, 500, and 900 mm depth were 0.91, 0.80, and 0.78 respectively. Although the model performance slightly declined with soil depth, overall the model provided satisfactory results in simulating soil moisture at different soil depths. Although considering the hydraulic conductivities anisotropy provides more flexibility and helps to improve the model fit, it was not imposed a priori in the calibration process but automatically selected so as to provide a better fit than in the isotropic case.

In terms of slope stability, Figure 9 presents the evolution of the probability of failure at 100, 500, and 900 mm depth and the measured rainfall for the entire

simulation period. The fact that the failure probability is lower than 1 confirmed that no landslides occurred at the measurement station location in the simulation period. The failure probability in the upper layers (100 and 500 mm) is much more sensitive to rainfall (hence soil moisture) variation compared to the deeper layer (900 mm). The zone located at 500 mm depth tends to be more prone to failure. At this depth the failure probability assumes high values in the wetter periods (around 0.80) and low values in the dry season (around 0.58). The zones located at 100 and 900 mm depth tend to be more stable. This could be explained by the fact that at 100 mm depth the combined effect of i) soil suction absolute values decreasing and ii) soil column weight increasing is not high enough to cause instability whereas at 900 mm depth the soil friction angle (of 30 degree) is high enough to ensure the soil stability.

Although the optimal model parameter set based on one monitoring point located in the upper part of the basin can be considered not fully representative of the entire area, it can be justified by: i) the small size (5 km2) of the analyzed domain and ii) the interest in modeling the triggering processes of the landslide which usually occur where the monitoring point is located. Finally, it should be stressed that the previous considerations are strictly related to the hydrological year we considered in the simulation period (2009) and to the analyzed study site. They cannot be treated as general and extended to other locations because the Sarno area is known to experience strong heterogeneities in terms of meteorological conditions, soil stratigraphy and soil parameter values.

5. Conclusions

An analysis was carried out at two different test sites to investigate the impact of soil hydraulic conductivity anisotropy on partially saturated, transient hydrology and slope stability at catchment scale. The analysis was based on the three-dimensional hydrological/slope stability model GEOtop-FS 2.0 which solves the coupled Richards and energy budget equations. The model is connected to an infinite slope stability module and it provides at different soil depths maps of soil moisture (or pressure heads) and the probability of failure. In the first test case the effect of soil hydraulic conductivity anisotropy is evaluated in a simulation framework on real morphologies (concave, convex, and planar) extracted from a 10m real elevation model. The increase in the anisotropy ratio (r=2 and r=10) anticipates the failure time in all three morphologies compared to the case of r=1. Moreover, for the concave morphology the instability involves more soil layers (wider unstable area) than concave and planar morphologies. The second case study integrated the model GEOtop-FS 2.0 and a field campaign carried out in the Tuostolo river basin in the Sarno area (South Italy). The availability of measured soil moisture data at different soil depth allowed automatic calibration of the soil parameters such as soil hydraulic conductivity (both normal and lateral) and soil water retention functions. The estimated optimal parameter set was used to estimate the evolution of failure probability at different depths. The model predicted no failure for the simulation period; the most unstable area was found at a depth of 500 mm, attaining a failure probability of around 0.80 in wet periods.

Results from the two case studies indicate that when rainfall infiltrates the soil

there is a decrease in soil shear strength due to a decrease in negative pore-water pressure. As a consequence, the probability of having a potential failure increases. When the hydraulic conductivity anisotropy ratio increases there is an increase in soil water mobility in the horizontal direction, inducing a decrease in the soil safety factor.

In line with other previous studies (such as Yeh et al., 2015) it can be concluded that at relatively low hydraulic conductivity anisotropy ratios (less than 10) the wetting front of the water infiltrating the soil is deeper and water reaches the groundwater table earlier, triggering possible instability conditions. This process also depends on soil geomorphology: the concave morphology tends to reach instability conditions before planar or convex morphologies for the same hydraulic conductivity anisotropy conditions.

Although soils presenting high hydraulic conductivity anisotropy ratios or different rainfall intensities could be investigated in greater depth, we demonstrated that soil hydraulic anisotropy can play a major role in slope stability. This can be well captured in physically based landslide prediction models which in turn we hope can soon be included in the landslide early-warning system chain.

Future work to improve the presented analysis includes the need for spatially variable quantification of the geo-mechanical properties of the soil, especially for soil strength parameters. In many cases slope stability can be very sensitive to soil strength and the hypothesis of considering a constant value for the entire area can often not be satisfied, especially for applications in larger basins. Measurements of soil hydrological and mechanical properties at deeper soil depths as well as a distributed network of soil moisture

measurement stations in the basin would be very important to improve model parameter estimation throughout the entire soil column and in more extensive areas. Among the limitations of the current analysis there is the model validation in the saturated zone, due to the lack of saturated pore water pressure measurements available in the study sites. Moreover, the implementation of more complex slope stability methods which better accounts for other effects on slope stability (e.g. buoyancy) will extend the application of the proposed framework for landslides with more complex sliding surface geometry such as rotational. Finally, there remain open questions regarding: i) quantification of model parameter uncertainty when calibrating complex environmental models and ii) addressing/reducing equifinality, i.e. many different parameter sets can lead to the same optimum value (equifinality, von Bertalanffy, 1968; Beven, 2006).

Tables

Table 1: Soil water retention curve and soil hydraulic conductivity function parameters for application 1. n [-] and α [1/m] are van Genuchten parameters, θ_r and θ_s are the residual and saturated water content, K_v[m/s] is the slope normal saturated hydraulic conductivity, $r = K_h / K_v$ is the soil anisotropy ratio, and K_h[m/s] is the lateral saturated hydraulic conductivity.

n [-]	α [1/m]	θ_r[-]	θ_s[-]	K_v[m/s]	$r = K_h / K_v$
					1

3.5	0.97	0.02	0.40	10^{-5}	2
					10

Table 2: Optimal parameter set for application 2 estimated in the calibration period for different soil layers (in bold) and soil mechanical parameters (friction angle and effective cohesion) used to calculate failure probability.

	Unit	Top soil	Pumice 1631 AD	Paleosoil type 1	Pumice 472 A.D	Paleosoil type 2	Bedrock
Depth	[mm]	600.0	350.0	500.0	350.0	450.0	200.0
Residual soil water content	[-]	**0.08**	**0.05**	**0.03**	**0.04**	**0.02**	**0.03**
Saturated soil water content	[-]	**0.45**	**0.6**	**0.5**	**0.55**	**0.48**	**0.5**
Normal saturated hydraulic conductivity	[m/s]	**8.00E-5**	**1.20E-3**	**2.00E-5**	**1.00E-3**	**5.00E-6**	**4.00E-6**
Lateral saturated hydraulic conductivity	[m/s]	**1.00E-4**	**2.80E-3**	**5.00E-5**	**2.20E-3**	**1.40E-5**	**6.00E-6**
a Van Genuchten	[1/kPa]	**0.4**	**8.0**	**2.2**	**6.0**	**2.2**	**2.5**
n Van Genuchten	[-]	**1.6**	**1.8**	**1.7**	**1.8**	**2**	**2.2**
Friction angle	[°]	15.0	30.0	25.0	32.0	28.0	21.0
Effective cohesion	kPa	2.0	0.0	4.5	0.0	4.7	15.0
Soil saturated unit weight	kN/m3	17.2	13.0	13.0	13.0	15.0	15.3

Figures

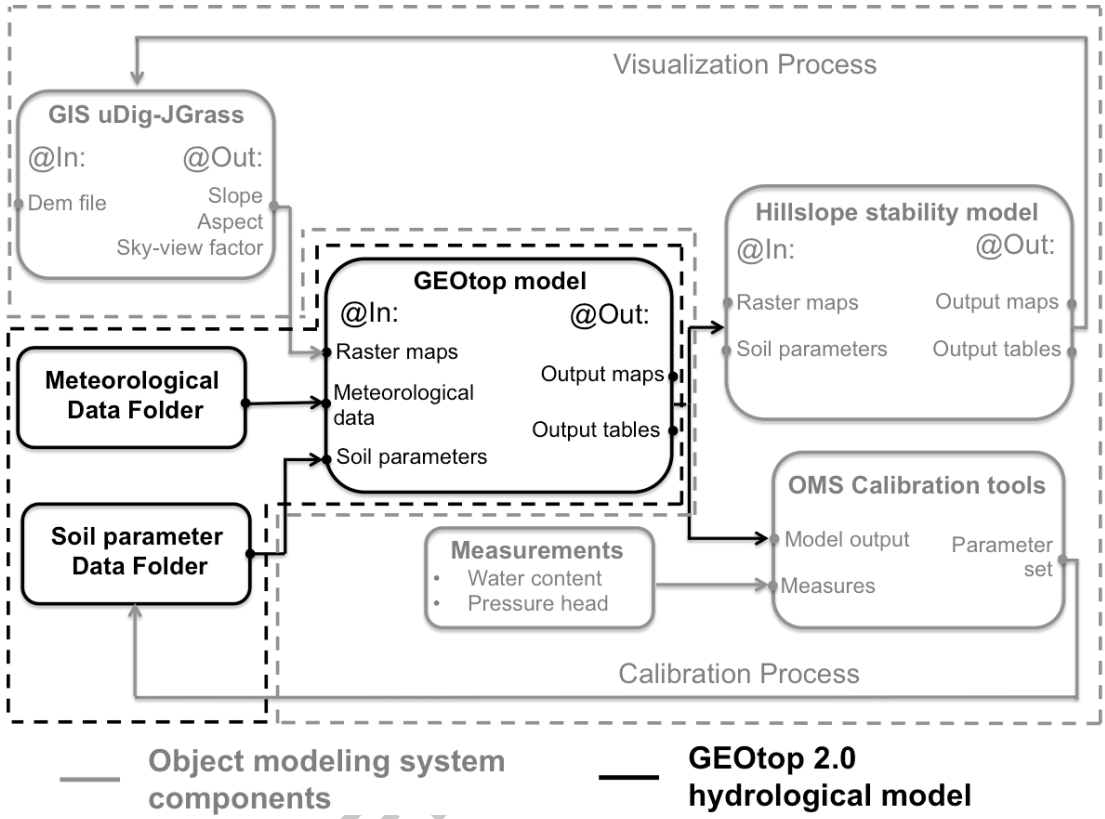

Figure 1: The GEOtop-FS 2.0 modeling framework: the hydrological model components are presented in black and the Object modeling system components in gray (Figure adapted from Formetta et al., 2016a).

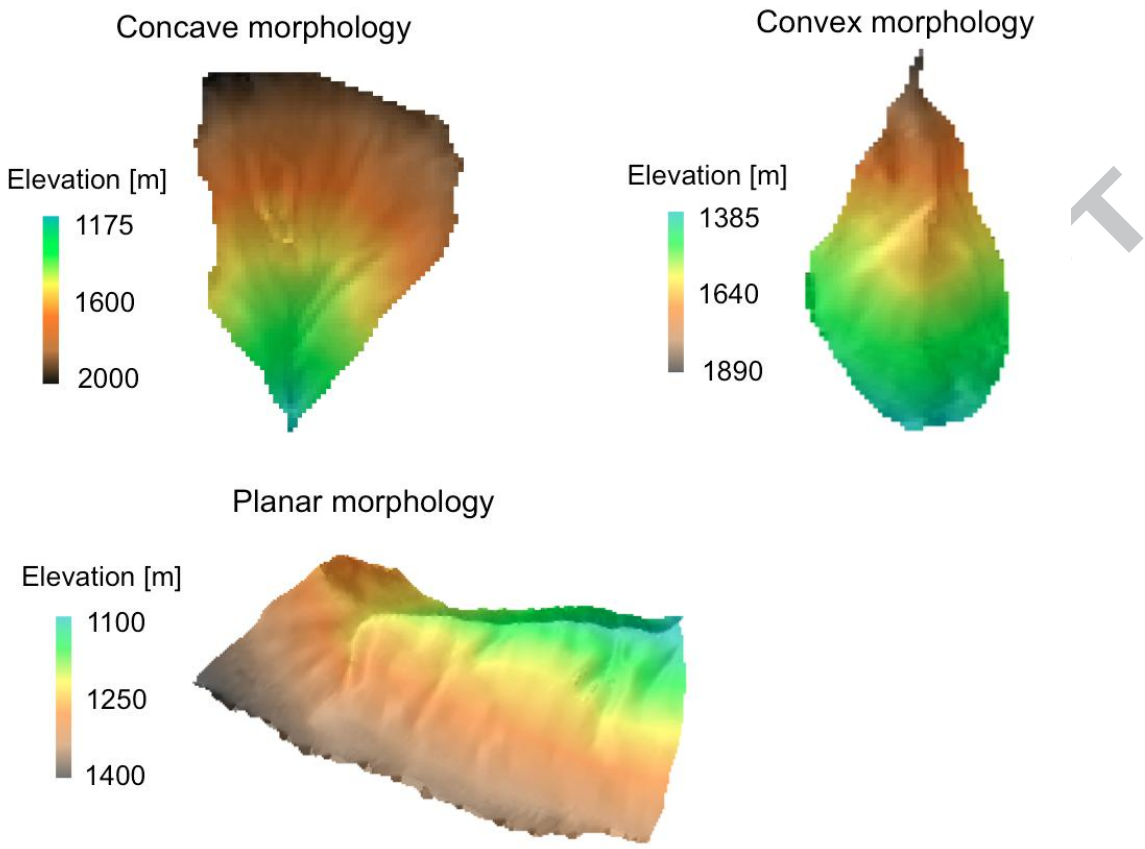

Figure 2: Digital elevation model of the three morphologies (concave, convex, and planar) of application 1.

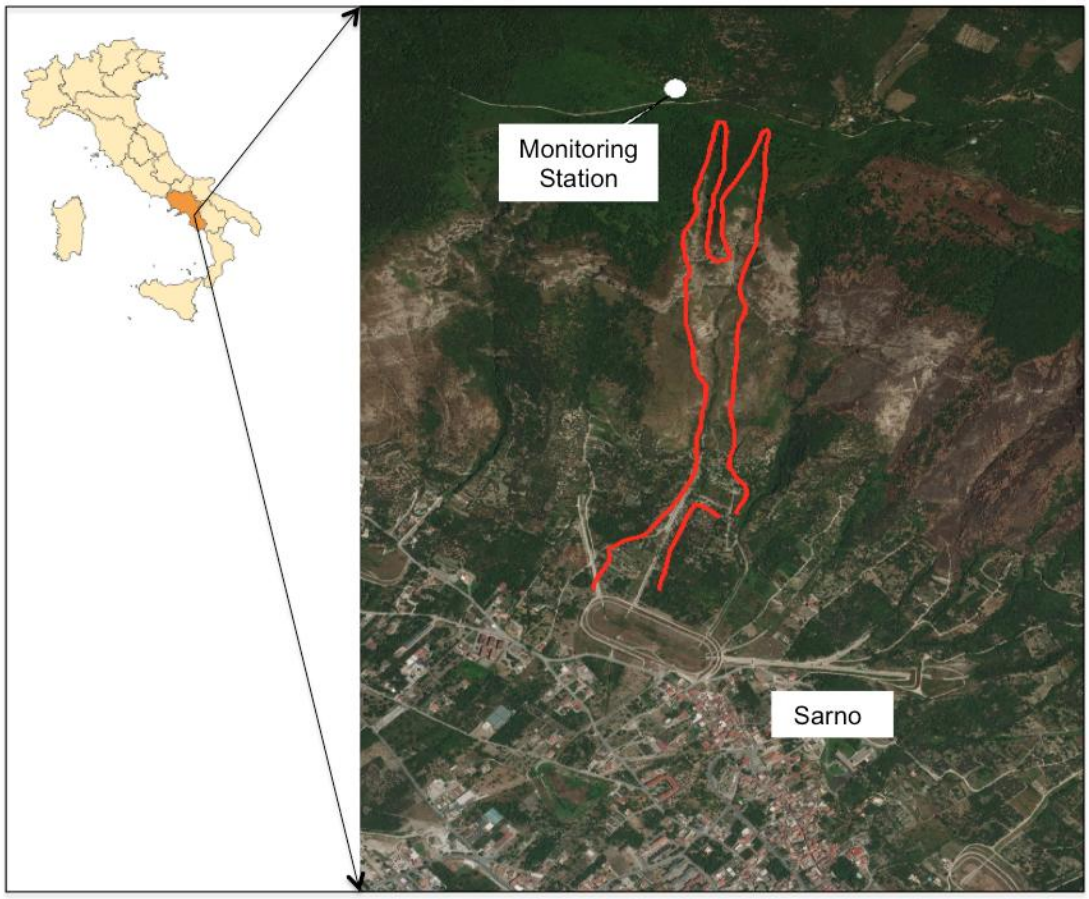

Figure 3: Study area for application 2. left) location of Sarno in southern of Italy – right) detail of the area where the monitoring station is located (40.846414 N, 14.608596 E and 760 m asl.) the red line indicates the shape of the mud flows occurred on May 5th, 1998

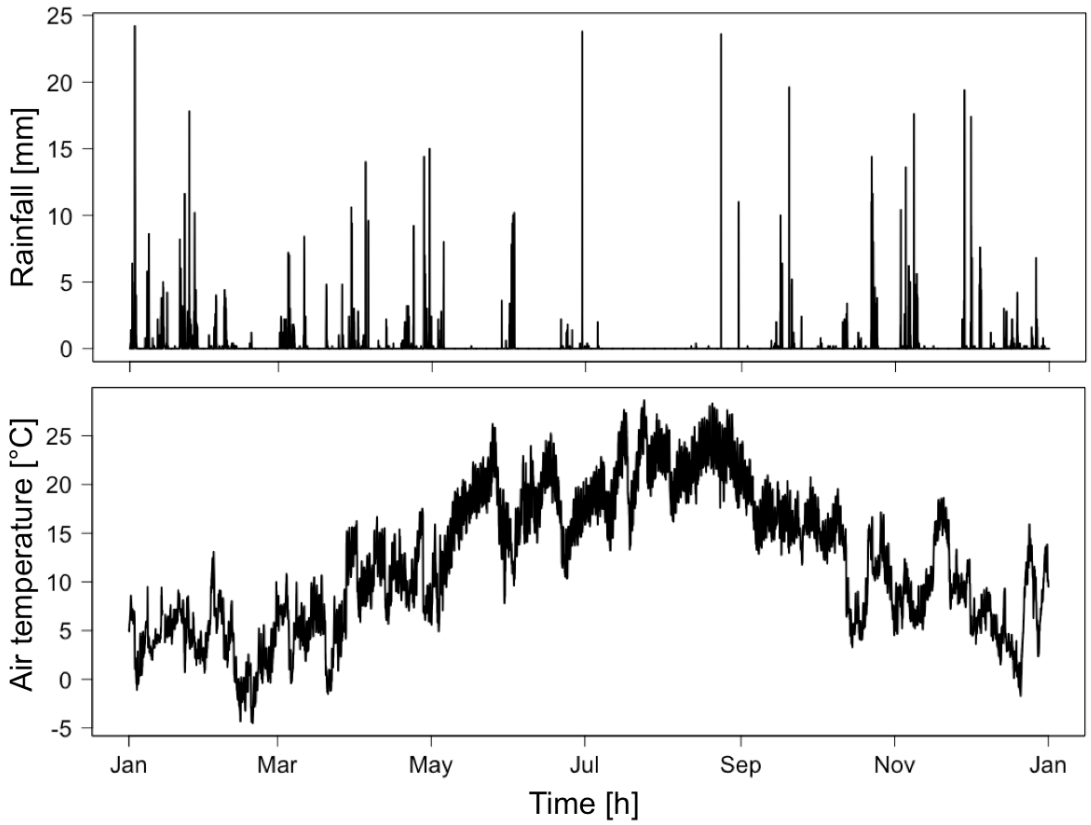

Figure 4: Rainfall and air temperature time series measured at the monitoring station for the year 2009. Measures are presented at hourly time steps.

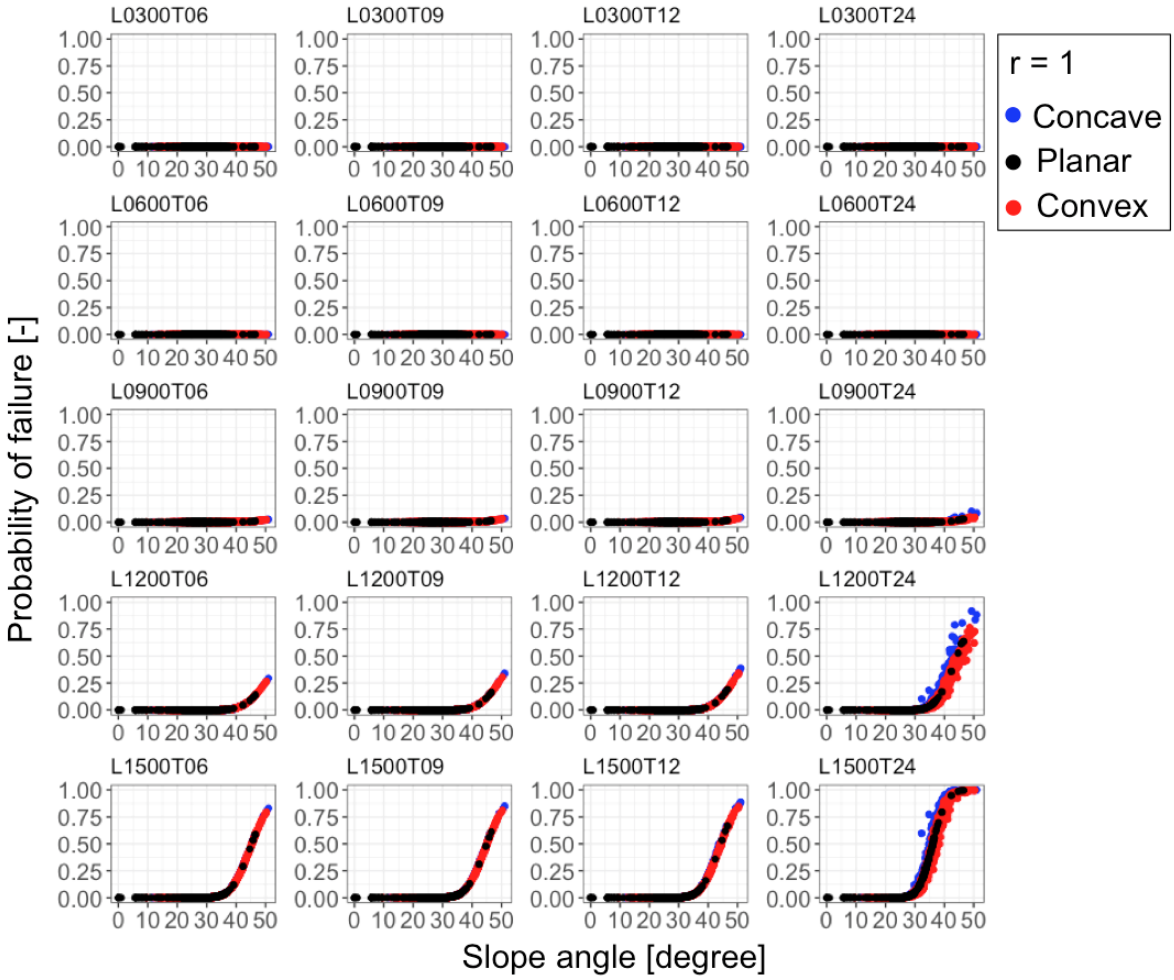

Figure 5: Evolution of the probability of failure as a function of slope for concave (blue), convex (red), and planar (black) morphologies and for anisotropy ratio r=1. Plots are provided for different soil layers (300, 900, 1200, and 1500 mm deep) and for different time steps (6, 9, 12, and 24, h from simulation start). Each row represents a given soil layer (label L stands for layer) and each column represents a given time step (label T stands for time after simulation start). Figure adapted from Formetta et al., 2016b

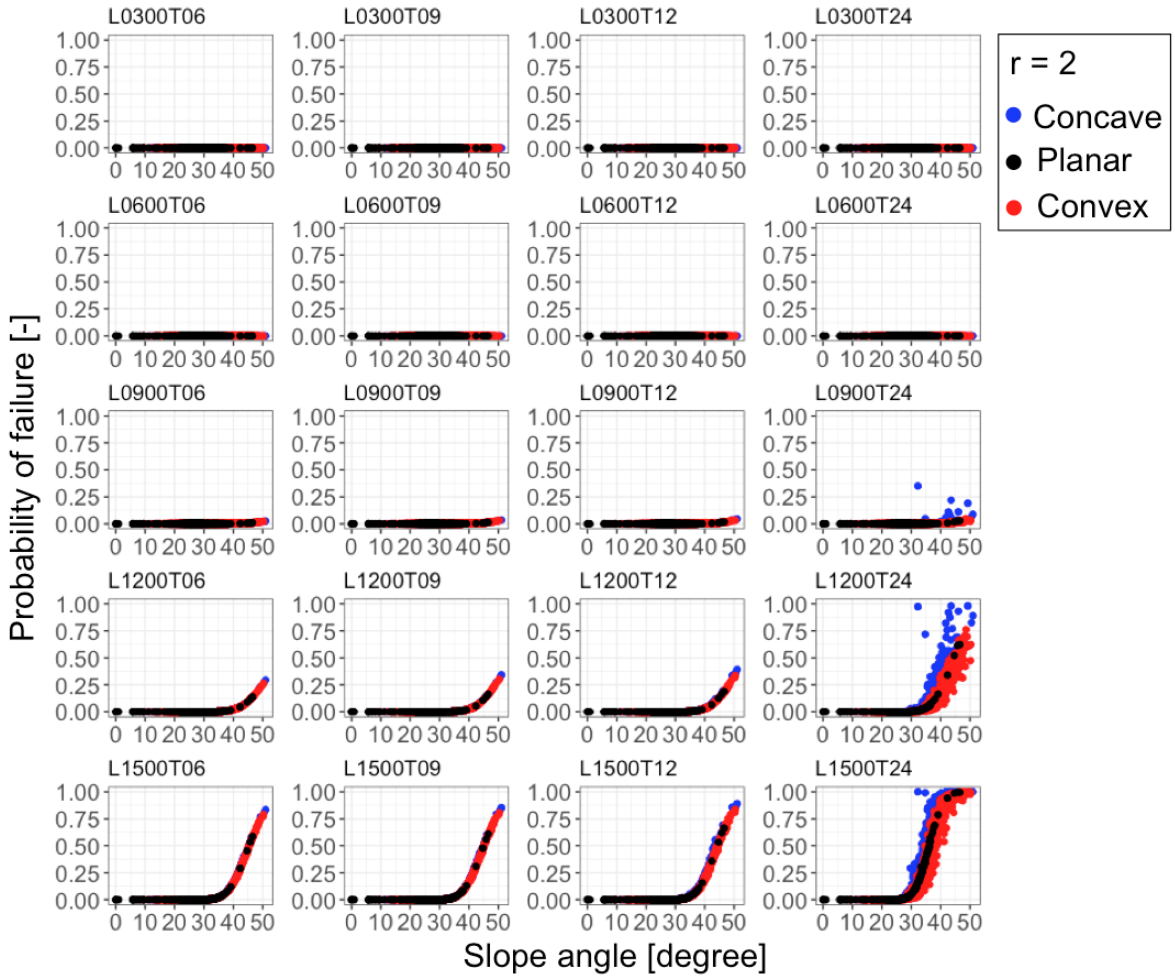

Figure 6: Evolution of the probability of failure as a function of slope for concave (blue), convex (red), and planar (black) morphologies and for anisotropy ratio r=2. Plots are provided for different soil layers (300, 900, 1200, and 1500 mm deep) and for different time steps (6, 9, 12, and 24, h from simulation start). Each row represents a given soil layer (label L stands for layer) and each column represents a given time step (label T stands for

time after simulation start).

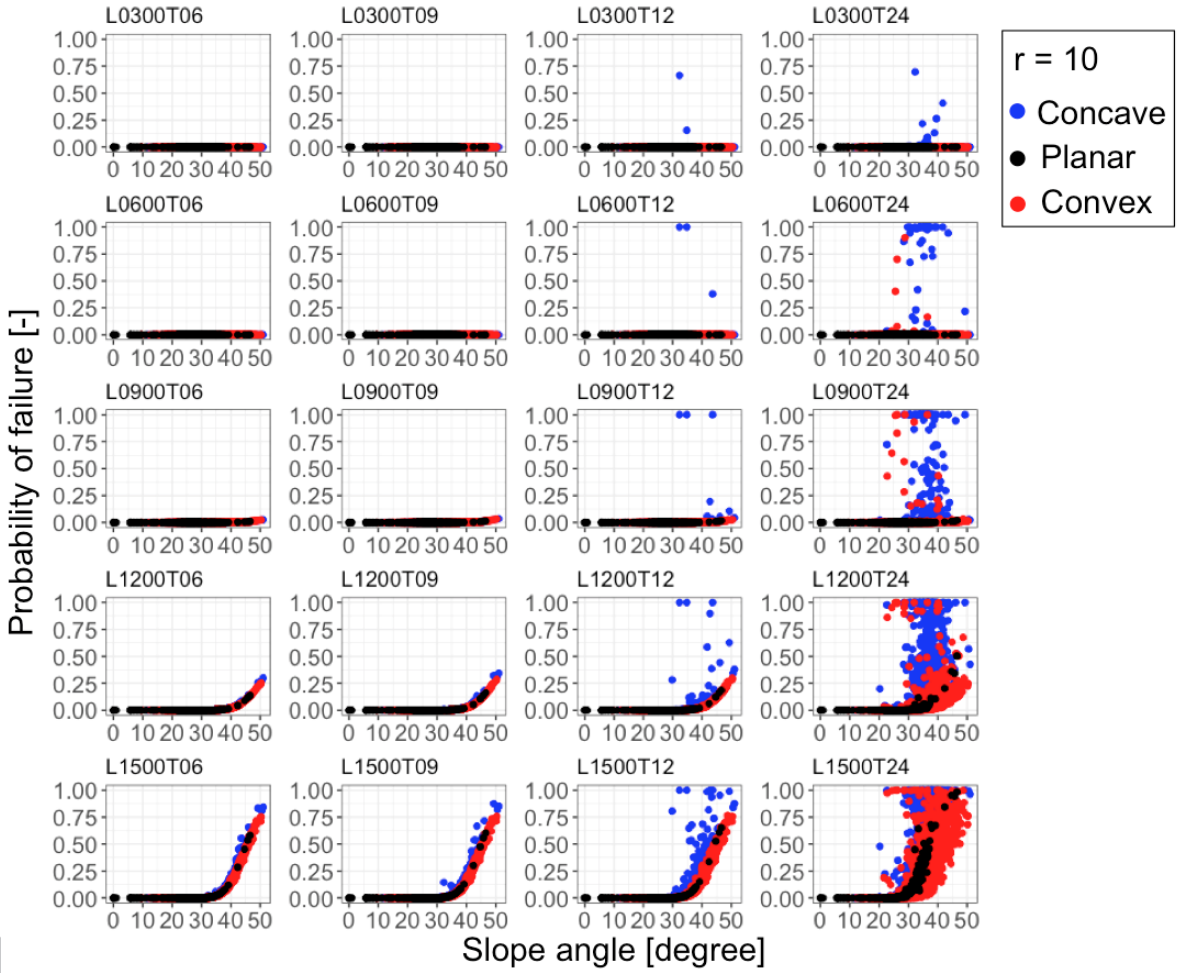

Figure 7: Evolution of the probability of failure as a function of slope for concave (blue), convex (red), and planar (black) morphologies and for anisotropy ratio r=10. Plots are provided for different soil layers (300, 900, 1200, and 1500 mm deep) and for different time steps (6, 9, 12, and 24, h from simulation start). Each row represents a given soil layer (label L stands

for layer) and each column represents a given time step (label T stands for time after simulation start).

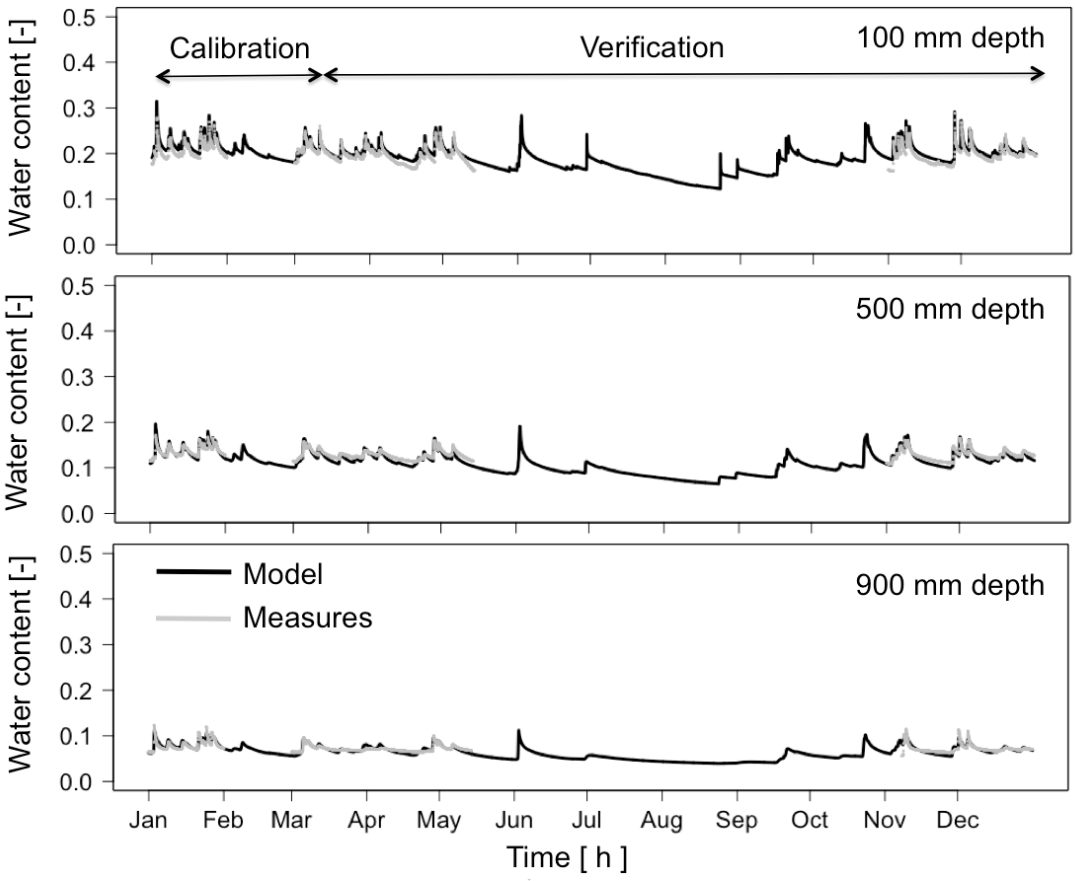

Figure 8: Simulated (in black) and measured (in gray) soil moisture time series at different soil depths (100, 500, and 900 mm) for the year 2009, for both calibration and validation periods.

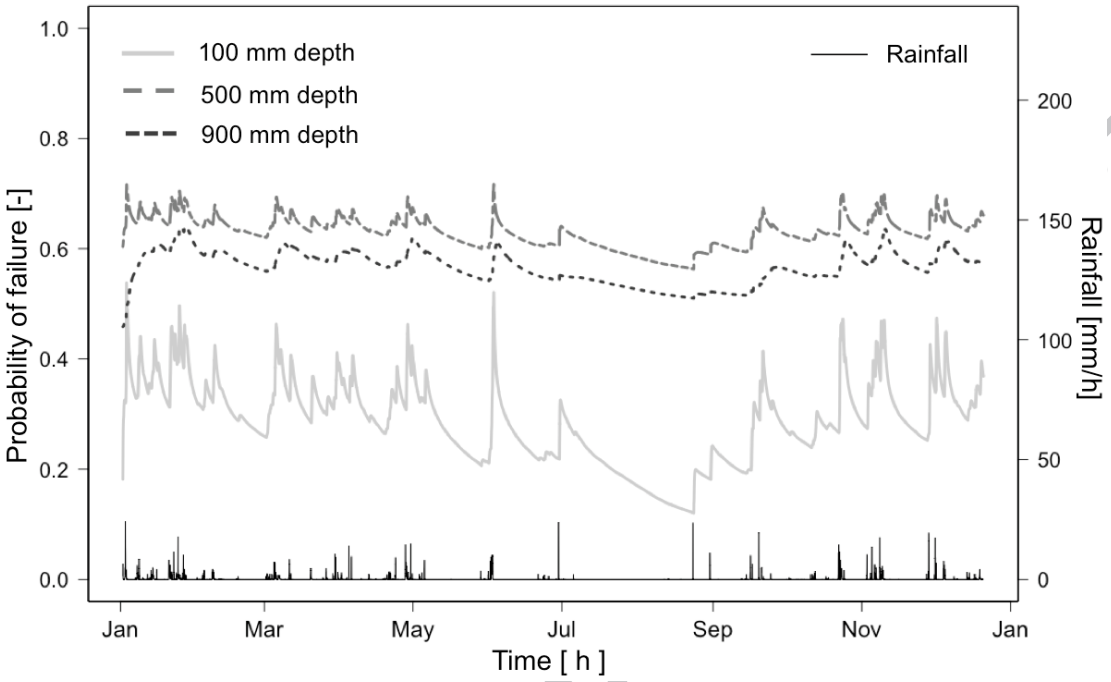

Figure 9: Evolution of the probability of failure at 100, 500, and 900 mm depth for the year 2009 in light gray, gray, and dark gray, respectively. The measured rainfall is presented in black.

Appendix 1: The geo-mechanical model component

The stability analyses of natural slopes require the evaluation of the destabilizing forces with respect to the shear strength of the soil and the variation of the shear strength itself (Lu and Godt, 2013). According to the general effective stress framework developed by Lu and Likos (2006) and Lu et al. (2010) the effective stress σ' [kPa] can be given as:

$$\sigma' = \sigma - u_a - \sigma^s \quad \text{(A1)}$$

where σ [kPa] is the total stress, u_a [kPa] is the pore air pressure, and σ^s [kPa] is the suction stress (Lu and Likos, 2004). The latter represents all the inter-particle stresses such as capillary stress, the electric double-layer force, the van der Waals attractive force and the matric suction of soil, and is defined as in Lu and Likos (2004):

$$\begin{aligned} \sigma^s &= -(u_a - u_w) && if\ (u_a - u_w) \le 0 \\ \sigma^s &= -\frac{\theta - \theta_r}{\theta_s - \theta_r} \cdot (u_a - u_w) && if\ (u_a - u_w) > 0 \end{aligned} \quad \text{(A2)}$$

where u_w [kPa] is the pore water pressure, θ is the volumetric water content, θ_r is the residual volumetric water content, and θ_s is the saturated volumetric water content. The general effective stress framework unifies the description of flow and stress phenomena in all types of soils, ranging from sand and silt to clay. Also, it does not require the definition of Bishop's effective stress parameter, given that suction stress is a function only of soil suction (Lu et al.

2010). Finally, the approach captures the nonlinear and peak behavior of the effective stress in sandy and silty soils (Lu and Likos, 2004, 2006).

The factor of safety FS (ratio of stabilizing to destabilizing forces) is computed by combining the generalized effective stress and strength failure criteria, for a uniform, infinite slope as expressed in Lu and Godt (2008) and Formetta et al. (2016):

$$FS = \frac{\tan\phi\prime}{\tan\beta} + \frac{c\prime}{\gamma \cdot Z \cdot sin\beta \cdot cos\beta} - \frac{\sigma^s \cdot \tan\phi\prime}{\gamma \cdot Z \cdot sin\beta \cdot cos\beta} \quad \text{(A3)}$$

where ϕ' [deg] is the effective internal friction angle, β [deg] is the slope angle, c' [kPa] is the cohesion at zero normal stress due to the intergranular bonding stress, γ $[kN/m^3]$ is the unit weight of soil, and Z [m] is the soil thickness. During a time-variant rainfall event the transient pressure heads influence the stress state of soil, inducing variations in suction stress. In particular, a decrease is caused in the absolute value of suction stresses, due to an increase in pressure head, which may induce shallow soil failure. Rainfall infiltration increases the water content and, as a consequence, the absolute values of both soil suction and suction stress decrease, making the slope more prone to failure (Lu and Godt, 2013; Formetta et al., 2016).

Assuming the friction angle, ϕ', and the cohesion coefficient, c', as random variables we state our interest in the probability of failure (i.e., the probability of FS) rather than in FS itself, as given by equation (A3). Assuming, therefore, that FS follows a lognormal distribution (Frattini et al., 2009; Duncan, 2000) the probability of failure is:

$$P[FS < 1] = P[\ln FS < 0] = \Phi\left(-\frac{\mu_{lnFS}}{\sigma_{lnFS}}\right) \quad \text{(A4)}$$

where Φ is the cumulative distribution function of the standard normal distribution;

$\mu_{lnFS} = (ln\,\mu_{FS} - 0.5 \cdot \sigma_{lnFS}^2)$; $\sigma_{lnFS} = \sqrt{ln(1+\nu_{FS}^2)}$; μ_{FS} and ν_{FS} are the mean and the coefficient of variation of FS computed using the First-Order Second Moment Method (FOSM) (Dai and Lee, 2002; Baecher and Christian, 2005; Formetta et al., 2016). The FOSM is used to approximate the expectation and variance of a function of independent random variables. The method approximates the desired statistic $G = G(x_1, \dots, x_n)$ with its Taylor series expansion about the expected values of random variables, such that:

$$E[G] = G(\mu[x_1], \dots, \mu[x_n]) \quad \text{(A5)}$$

$$\sigma^2[G] = \sum_{i=1}^{n}\left(\frac{dG}{dx_i} \cdot \sigma[x_i]\right)^2 \quad \text{(A6)}$$

where $\mu[x_i]$ and $\sigma[x_i]$ are, respectively, the mean and standard deviation of the random variable x_i. Soil friction angle and cohesion standard deviations are assumed as 40% and 10% of the mean, according to Fredlund and Dahlman (1972) and Lumb (1966), respectively. These assumption were tested elsewhere (Arnone et al., 2014; Formetta et al., 2016).

The model is run by using different soil moisture conditions and pressure heads computed for each time step by the three-dimensional hydrological model GEOtop. This provides an FS probability that varies in time and space.

The calculation is performed for each layer (into which the soil depth has been discretized) to investigate the stability at different depths, after characterizing the soil in geotechnical terms. Therefore FS probability also varies with depth, and the depth of a potential failure is allowed to vary from the surface to the bedrock without any constraint. The size of the unstable area is approximated by the number of pixels in the soil column with a failure probability higher than 0.9. Finally, the implementation of the infinite slope stability model suites the analyzed case studies where likely planar landslides occur in layered soils. Moreover, the method as it is implemented does not require any a priori assumption on the depth or shape of the failure surface.

Appendix 2

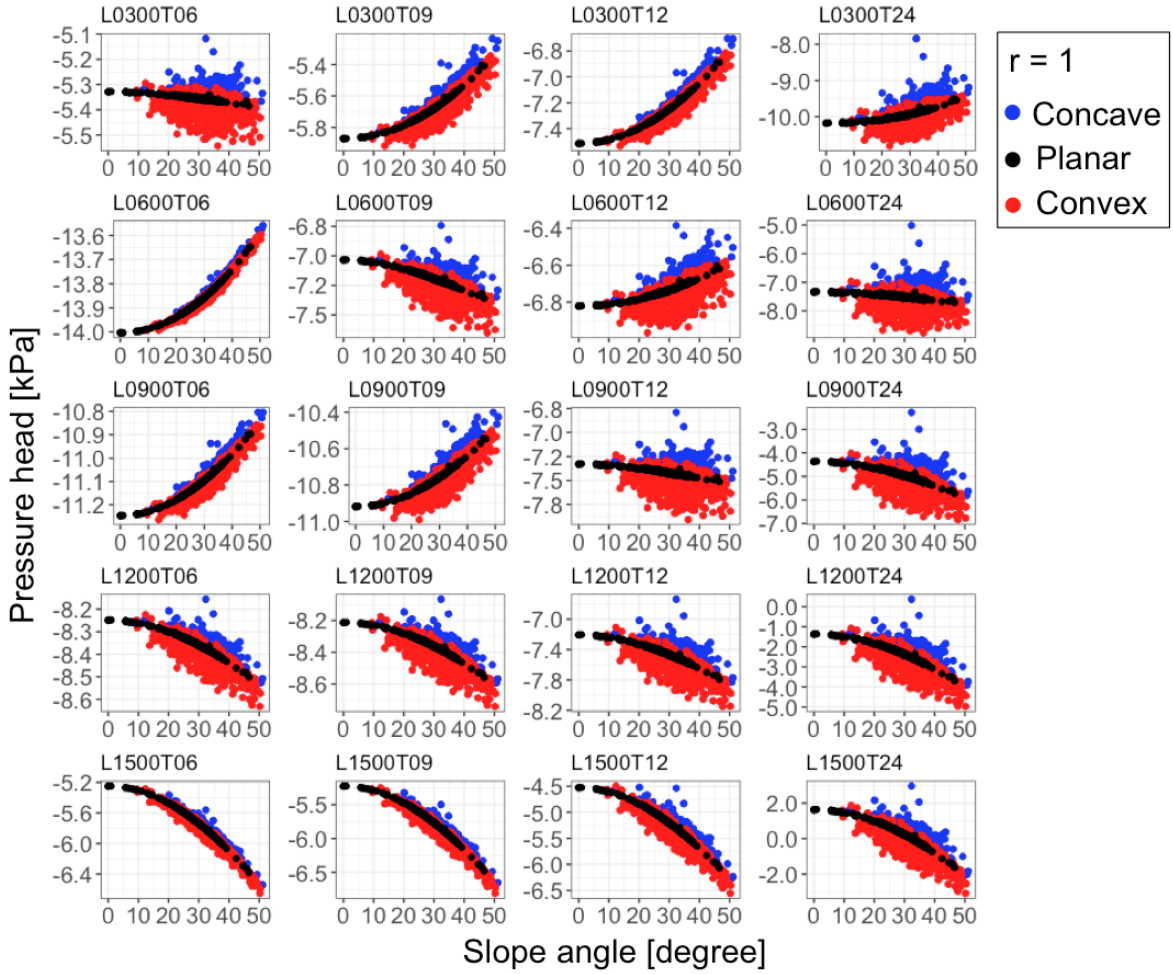

Figure A-1: Evolution of the pressure head as a function of slope for concave (blue), convex (red), and planar (black) morphologies and for anisotropy ratio r =1. Plots are provided for different soil layers (300, 900, 1200, and 1500 mm deep) and for different time steps (6, 9, 12, and 24, h from simulation start). Each row represents a given soil layer (label L stands for layer) and each column represents a given time step (label T stands for time after simulation start).

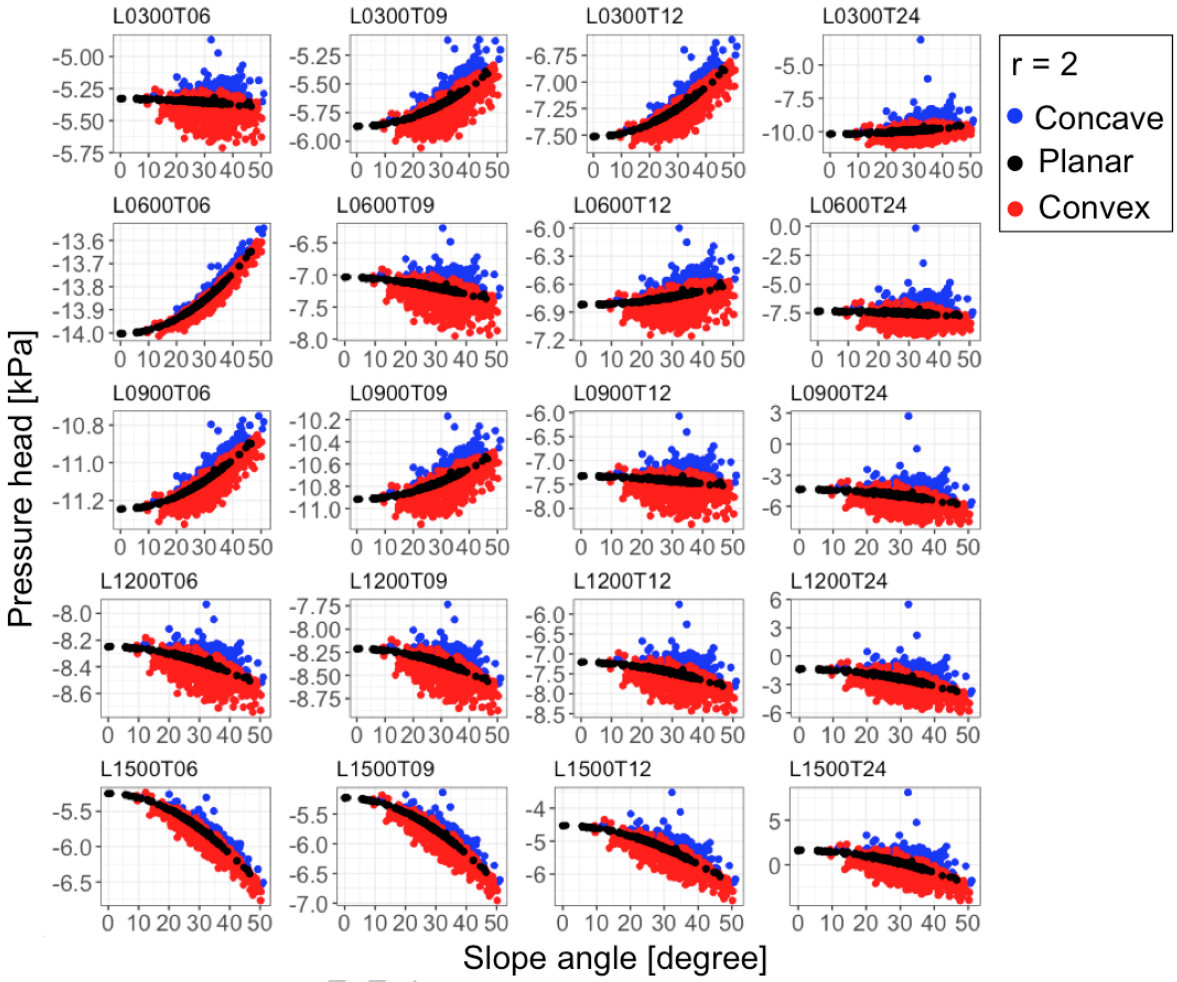

Figure A-2: Evolution of the pressure head as a function of slope for concave (blue), convex (red), and planar (black) morphologies and for anisotropy ratio r =2. Plots are provided for different soil layers (300, 900, 1200, and 1500 mm deep) and for different time steps (6, 9, 12, and 24, h from simulation start). Each row represents a given soil layer (label L stands for layer) and each column represents a given time step (label T stands for time after simulation start).

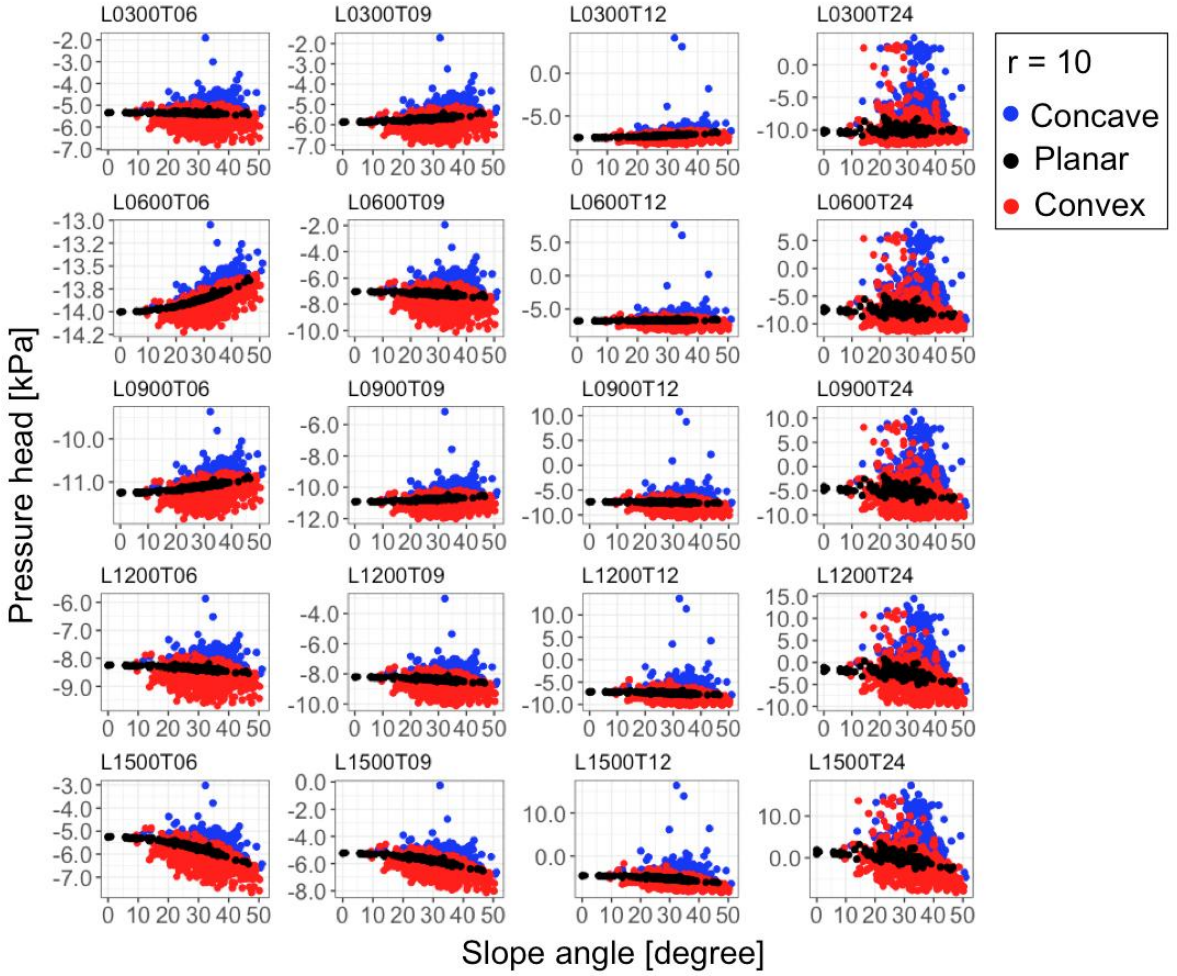

Figure A-3: Evolution of the pressure head as a function of slope for concave (blue), convex (red), and planar (black) morphologies and for anisotropy ratio r =10. Plots are provided for different soil layers (300, 900, 1200, and 1500 mm deep) and for different time steps (6, 9, 12, and 24, h from simulation start). Each row represents a given soil layer (label L stands for layer) and each column represents a given time step (label T stands for time after simulation start).

References

Abera, W., Antonello, A., Franceschi, S., Formetta, G., & Rigon, R. (2014). The uDig Spatial Toolbox for hydro-geomorphic analysis. Geomorphological Techniques, 2(4.1), 1-19.

Abera, W., Formetta, G., Borga, M., & Rigon, R. (2017). Estimating the water budget components and their variability in a pre-alpine basin with JGrass-NewAGE. Advances in Water Resources, 104, 37-54.

Abera, W., Formetta, G., Brocca, L., & Rigon, R. (2017). Modeling the water budget of the Upper Blue Nile basin using the JGrass-NewAge model system and satellite data. Hydrology and Earth System Sciences, 21(6), 3145.

Affuso AM, Casagli N, Dapporto S, Gabbani G, Gargini A, Rinaldi M (2000) Monitoring and modeling of unsaturated flow and effects on streambank failures. In Bromhead E, Dixon N, Ibsen ML (eds) Landslides, in research, theory and practice. Proceedings of the 8th International Symposium on Landslides, 26–30 June 2000, Cardiff, pp 7–12

An, H., Viet, T. T., Lee, G., Kim, Y., Kim, M., Noh, S., & Noh, J. (2016). Development of time-variant landslide-prediction software considering three-dimensional subsurface unsaturated flow. Environmental modelling & software, 85, 172-183.

Arnalds, Ó., Bartoli, F., Buurman, P., García-Rodeja, E., Óskarsson, H., & Stoops, G. (Eds.). (2007). Soils of volcanic regions in Europe (p. 644). Berlin: Springer.

Baecher, G. B., & Christian, J. T. (2005). Reliability and statistics in geotechnical engineering. John Wiley & Sons.

Barling, R. D., Moore, I. D., & Grayson, R. B. (1994). A quasi- dynamic wetness index for characterizing the spatial distribution of zones of surface saturation and soil water content. Water Resources Research, 30(4), 1029-1044.

Baum, R. L., Godt, J. W., & Savage, W. Z. (2010). Estimating the timing and location of shallow rainfall- induced landslides using a model for transient, unsaturated infiltration. Journal of Geophysical Research: Earth Surface, 115(F3).

Bertoldi, G., Rigon, R., & Over, T. M. (2006). Impact of watershed geomorphic characteristics on the energy and water budgets. Journal of Hydrometeorology, 7(3), 389-403.

Beven, K. (2006). A manifesto for the equifinality thesis. Journal of hydrology, 320(1-2), 18-36.

Bishop, A. W. (1955), The use of slip circle in the stability analysis of slopes,Geotechnique,5(1), 7–17, doi:10.1680/geot.1955.5.1.7.

Borga, M., Dalla Fontana, G., & Cazorzi, F. (2002). Analysis of topographic and climatic control on rainfall-triggered shallow landsliding using a quasi-dynamic wetness index. Journal of Hydrology, 268(1-4), 56-71.

Capparelli, G., & Versace, P. (2011). FLaIR and SUSHI: two mathematical models for early warning of landslides induced by rainfall. Landslides, 8(1), 67-79.

Capparelli, G., & Versace, P. (2014). Analysis of landslide triggering conditions in the Sarno area using a physically based model. Hydrology and Earth System Sciences, 18(8), 3225.

Carrara, A., Guzzetti, F., Cardinali, M., & Reichenbach, P. (1999). Use of GIS technology in the prediction and monitoring of landslide hazard. Natural hazards, 20(2-3), 117-135.

Cascini, L., Cuomo, S., & Della Sala, M. (2011). Spatial and temporal occurrence of rainfall-induced shallow landslides of flow type: A case of Sarno-Quindici, Italy. Geomorphology, 126(1), 148-158.

Castiglioni G. 1962. L'erosione attuale nella conca di Sauris (Carnia), Aspetti geografici dell'erosione del suolo in Italia. CNR Centro di Studiper Geografia fisica: Carnia; 199–220.

Chen, P., Mirus, B., Lu, N., & Godt, J. W. (2017). Effect of hydraulic hysteresis on stability of infinite slopes under steady infiltration. Journal of Geotechnical and Geoenvironmental Engineering, 143(9), 04017041.

Corominas, J., Van Westen, C., Frattini, P., Cascini, L., Malet, J. P., Fotopoulou, S., ... & Pitilakis, K. (2014). Recommendations for the quantitative analysis of landslide risk. Bulletin of engineering geology and the environment, 73(2), 209-263.

Dai, F. C., Lee, C. F., & Ngai, Y. Y. (2002). Landslide risk assessment and management: an overview. Engineering geology, 64(1), 65-87.

Damiano, E., Greco, R., Guida, A., Olivares, L., & Picarelli, L. (2017). Investigation on rainwater infiltration into layered shallow covers in pyroclastic soils and its effect on slope stability. Engineering Geology, 220, 208-218.

Del Prete M, Guadagno FM, Hawkins AB (1998) Preliminary report on the landslides of 5 May 1998, Campania, southern Italy. Bull Eng Geol Environ 57(2):113–129

De Vita P, Napolitano E, Godt J, Baum R. 2013. Deterministic estimation of hydrological thresholds for shallow landslide initiation and slope stability models: case study from the Somma-Vesuvius area of southern Italy. Landslides, 10, 713-728, DOI 10.1007/s10346-012-0348-2.

De Vita, P., & Piscopo, V. (2002). Influences of hydrological and hydrogeological conditions on debris flows in peri-vesuvian hillslopes. Natural Hazards and Earth System Science, 2(1/2), 27-35.

Di Crescenzo, G., & Santo, A. (2005). Debris slides–rapid earth flows in the carbonate massifs of the Campania region (Southern Italy): morphological and morphometric data for evaluating triggering susceptibility. Geomorphology, 66(1), 255-276.

Dietrich, W. E., Reiss, R., Hsu, M. L., & Montgomery, D. R. (1995). A process- based model for colluvial soil depth and shallow landsliding using digital elevation data. Hydrological processes, 9(3- 4), 383-400.

Dong JJ, Hsu HH (2011) Effects of hydraulic conductivity/strength anisotropy on the stability of stratified, poorly cemented rock slopes. Geophys Res 13:EGU2011-1953

Endrizzi, S., Gruber, S., Dall'Amico, M., & Rigon, R. (2014). GEOtop 2.0: simulating the combined energy and water balance at and below the land surface accounting for soil freezing, snow cover and terrain effects. Geoscientific Model Development, 7(6), 2831-2857.

Esposito E, Porfido S, Violante C, Biscardini C, Alaia F, Esposto G (2004) Water events and historical flood recurrences in the Vietri sul Mare coastal area (Costiera Amalfitana, southern Italy). Int Assoc Hydrol Sci (IAHS) 286:95–106

Fellenius, W. (1936), Calculation of the stability of earth dams, inTransactions of the 2nd Congress on Large Dams, vol. 4, pp. 445–463,Int. Comm. on Large Dams, Washington, D.C

Formetta, G.; Mantilla, R.; Franceschi, S.; Antonello, A.; Rigon, R. The JGrass-Newage system for forecasting and managing the hydrological

budgets at the basin scale: Models of flow generation and propagation/routing. Geosci. Model Dev. 2011, 4, 943–955.

Formetta, G.; Rigon, R.; Chávez, J.L.; David, O. Modeling shortwave solar radiation using the JGrass-NewAge system. Geosci. Model Dev. 2013, 6, 915–928.

Formetta, G.; Antonello, A.; Franceschi, S.; David, O.; Rigon, R. Hydrological modelling with components: A GIS-based open-source framework. Environ. Model. Softw. 2014, 55, 190–200

Formetta, G., Kampf, S. K., David, O., and Rigon, R.: Snow water equivalent modeling components in NewAge-JGrass, Geosci. Model Dev., 7, 725-736, https://doi.org/10.5194/gmd-7-725-2014, 2014.

Formetta, G., Bancheri, M., David, O., and Rigon, R.: Performance of site-specific parameterizations of longwave radiation, Hydrol. Earth Syst. Sci., 20, 4641-4654, https://doi.org/10.5194/hess-20-4641-2016, 2016.

Formetta, G., Rago, V., Capparelli, G., Rigon, R., Muto, F., & Versace, P. (2014). Integrated Physically based system for modeling landslide susceptibility. Procedia Earth and Planetary Science, 9, 74-82.

Formetta, G., Simoni, S., Godt, J. W., Lu, N., & Rigon, R. (2016). Geomorphological control on variably saturated hillslope hydrology and slope instability. Water Resources Research, 52(6), 4590-4607.

Formetta, G., Capparelli, G., & Versace, P. (2016). Evaluating performance of simplified physically based models for shallow landslide susceptibility. Hydrology and Earth System Sciences, 20(11), 4585-4603.

Frattini, P., Crosta, G. B., Fusi, N., & Dal Negro, P. (2004). Shallow landslides in pyroclastic soils: a distributed modelling approach for hazard assessment. Engineering Geology, 73(3-4), 277-295.

Frattini, P., Crosta, G., and Carrara, A.: Techniques for evaluating the performance of landslide susceptibility models, Eng. Geol., 111, 62–72, 2010.

Fusco F, P De Vita, V Allocca. 2017. Hydro-geomorphological modelling of ash-fall pyroclastic soils for debris flow initiation and groundwater recharge in Campania (southern Italy). Catena, 158 (2017) 235-249, doi:10.1016/j.catena.2017.07.010

Gardner, W. R. (1958). Some steady-state solutions of the unsaturated moisture flow equation with application to evaporation from a water table. Soil science, 85(4), 228-232.

Gioia, E., Speranza, G., Ferretti, M., Godt, J. W., Baum, R. L., and Marincioni, F.: Application of a process-based shallow landslide hazard model over a

broad area in Central Italy, Landslides, 13, 1197–1214, https://doi.org/10.1007/s10346-015-0670-6, 2016.

Gottardi, G., & Venutelli, M. (1993). A control-volume finite-element model for two-dimensional overland flow. Advances in water resources, 16(5), 277-284.

Gupta, H. V., Kling, H., Yilmaz, K. K., & Martinez, G. F. (2009). Decomposition of the mean squared error and NSE performance criteria: Implications for improving hydrological modelling. Journal of Hydrology, 377(1-2), 80-91.

Guzzetti, F., Carrara, A., Cardinali, M., & Reichenbach, P. (1999). Landslide hazard evaluation: a review of current techniques and their application in a multi-scale study, Central Italy. Geomorphology, 31(1), 181-216.
Hillel, D.: Fundamentals of soil physics, Academic Press, New York, NY, USA, 1980.

Guzzetti, F., Reichenbach, P., Ardizzone, F., Cardinali, M., and Galli, M.: Estimating the quality of landslide susceptibility mod- els, Geomorphology, 81, 166–184, 2006.

Hay, L. E., Leavesley, G. H., Clark, M. P., Markstrom, S. L., Viger, R. J., & Umemoto, M. (2006). STEP WISE, MULTIPLE OBJECTIVE CALIBRATION OF A HYDROLOGIC MODEL FOR A SNOWMELT DOMINATED BASIN 1. JAWRA Journal of the American Water Resources Association, 42(4), 877-890.

Hong, Y., Adler, R., & Huffman, G. (2006). Evaluation of the potential of NASA multi- satellite precipitation analysis in global landslide hazard assessment. Geophysical Research Letters, 33(22).

International Federation of Red Cross and Red Crescent Societies (2003). Personnel (local staff), 1(754,274), 754-274.

Itasca, F. L. A. C. (2000). Fast Lagrangian analysis of continua. Itasca Consulting Group Inc., Minneapolis, Minn.

Iverson, R. M., Denlinger, R. P., LaHusen, R. G., & Logan, M. (2000). Two-phase debris-flow across 3-D terrain: model predictions and experimental tests. In Debris-flow hazards mitigation: mechanics, prediction, and assessment.

Iverson, R.,M. Reid, and R. LaHusen (1997), Debris-flow mobilization from landslides, Annual Review of Earth and Planetary Sciences, 25, 85–138.

Janbu, N. (1973), Slope stability computations. Embankment-dam engineering, in Casagrande, vol. R, edited by C. Hirschfeld and S. J. Poulos,pp. 49–86, John Wiley, New York.

Kasim F, Fredlund DG, Gan JKM, Kay, Ho KKS (eds) (1998) The effect of steady state rainfall on long term matric suction conditions. Slope Engineering in Hong Kong, Balkema, pp 75–85

Keefer, D. K., & Larsen, M. C. (2007). Assessing landslide hazards. Science, 1136-1138.

Lanni, C., Borga, M., Rigon, R., & Tarolli, P. (2012). Modelling shallow landslide susceptibility by means of a subsurface flow path connectivity index and estimates of soil depth spatial distribution. Hydrology and Earth System Sciences, 16(11), 3959-3971.

Lepore, C., Arnone, E., Noto, L. V., Sivandran, G., & Bras, R. L. (2013). Physically based modeling of rainfall-triggered landslides: a case study in the Luquillo forest, Puerto Rico.

Lloyd, W., David, O., Ascough, J. C., Rojas, K. W., Carlson, J. R., Leavesley, G. H., & Ahuja, L. R. (2011). Environmental modeling framework invasiveness: Analysis and implications. Environmental modelling & software, 26(10), 1240-1250.
Lu, N., & Likos, W. J. (2006). Suction stress characteristic curve for unsaturated soil. Journal of geotechnical and geoenvironmental engineering, 132(2), 131-142.

Liston, G.E., Elder, K., 2006. A Meteorological Distribution System for High-Resolution Terrestrial Modeling (MicroMet). J. Hydromet. 7, 217–234.

Lu, N., & Godt, J. (2008). Infinite slope stability under steady unsaturated seepage conditions. Water Resources Research, 44(11).

Lu, N., B.Şener-Kaya, A. Wayllace, and J. W. Godt (2012), Analysis of rainfall-induced slope instability using a fieldof local factor of safety,Water Resour. Res.,48, W09524, doi:10.1029/2012WR011830

Lu, N., & Godt, J. W. (2013). Hillslope hydrology and stability. Cambridge University Press.

Matsui, T., and K. C. San (1992), Finite element slope stability analysis byshear strength reduction technique,Soil Found.,32(1), 59–70, doi:10.3208/sandf1972.32.59

Mergili, M., Emmer, A., Juřicová, A., Cochachin, A., Fischer, J. T., Huggel, C., & Pudasaini, S. P. (2018). How well can we simulate complex hydro- geomorphic process chains? The 2012 multi- lake outburst flood in the Santa Cruz Valley (Cordillera Blanca, Perú). Earth Surface Processes and Landforms.

Mirus, B. B., Ebel, B. A., Loague, K., & Wemple, B. C. (2007). Simulated effect of a forest road on near- surface hydrologic response: Redux. Earth

Surface Processes and Landforms: The Journal of the British Geomorphological Research Group, 32(1), 126-142.

Mirus, BB, K Perkins, JR Nimmo, K Singha. 2009. Hydrologic characterization of desert soils with varying degrees of pedogenesis: 2. Inverse modeling for effective properties. Vadose Zone Journal, doi:10.2136/vzj.2008.0051.

Mirus, B. B. (2015). Evaluating the importance of characterizing soil structure and horizons in parameterizing a hydrologic process model. Hydrological Processes, 29(21), 4611-4623.

Mirus, BB, J Smith, J Godt, R Baum, J Coe. 2016. Simulated Effect of Topography and Soil Properties on Hydrologic Response and Landslide Potential in the Oregon Coast Range, USA, in Aversa, S., Cascini, L., Picarelli, L., and Scavia, C., eds., Landslides and Engineered Slopes: Experience, Theory and Practice, CRC Press, Rome, Italy, ISBN 978-1-4987-8807, p. 1431-1439, doi:10.1201/b21520-176.

Montgomery, D. R., & Dietrich, W. E. (1994). A physically based model for the topographic control on shallow landsliding. Water resources research, 30(4), 1153-1171.

Morgenstern, N. R., and V. E. Price (1965), The analysis of the stability of general slip surface, Geotechnique,15(4), 289–290

Napolitano, E., Fusco, F., Baum, R. L., Godt, J. W., & De Vita, P. (2016). Effect of antecedent-hydrological conditions on rainfall triggering of debris flows in ash-fall pyroclastic mantled slopes of Campania (southern Italy). Landslides, 13(5), 967-983.

Ng, C. W. W., & Shi, Q. (1998). A numerical investigation of the stability of unsaturated soil slopes subjected to transient seepage. Computers and geotechnics, 22(1), 1-28.

Nimmo, JR, KS Perkins, KM Schmidt, JD Stock, DM Miller, and K Singha. 2009. Hydrologic characterization of desert soils with varying degrees of pedogenesis: 1. Field experiments evaluating plant-relevant soil water behavior. Vadose Zone Journal, doi:10.2136/vzj2008.0052.

Olivares, L., & Damiano, E. (2007). Postfailure mechanics of landslides: laboratory investigation of flowslides in pyroclastic soils. Journal of geotechnical and geoenvironmental engineering, 133(1), 51-62.

Orsi, G., Di Vito, M. A., & Isaia, R. (2004). Volcanic hazard assessment at the restless Campi Flegrei caldera. Bulletin of Volcanology, 66(6), 514-530.

Pack, R. T., Tarboton, D. G., & Goodwin, C. N. (1998, September). The SINMAP approach to terrain stability mapping. In 8th congress of the

international association of engineering geology, Vancouver, British Columbia, Canada (Vol. 21, p. 25).

Panday, S., & Huyakorn, P. S. (2004). A fully coupled physically-based spatially-distributed model for evaluating surface/subsurface flow. Advances in water Resources, 27(4), 361-382.

Park, H. J., Lee, J. H., & Woo, I. (2013). Assessment of rainfall-induced shallow landslide susceptibility using a GIS-based probabilistic approach. Engineering Geology, 161, 1-15.

Picarelli, L., Evangelista, A., Rolandi, G., Paone, A., Nicotera, M. V., Olivares, L., ... & Rolandi, M. (2006, December). Mechanical properties of pyroclastic soils in Campania Region. In Invited paper, 2nd Int. Workshop on Characterisation and Engineering Properties of Natural Soils, Singapore.

Revellino, P., Hungr, O., Guadagno, F. M., and Evans, S. G.: Velocity and runout simulation of destructive debris flows and debris avalanches in pyroclastic deposits, Campania region, Italy, Envi- ron. Geol., 45, 295–311, 2004.

Richards, L. A. (1931). Capillary conduction of liquids through porous mediums. physics, 1(5), 318-333.

Rigon, R., Bertoldi, G., & Over, T. M. (2006). GEOtop: A distributed hydrological model with coupled water and energy budgets. Journal of Hydrometeorology, 7(3), 371-388.

Rossi, F., Chirico, G.B., 1998. Definizione delle soglie pluviometriche d'allarme. G.N.D.C.I.-Dept. of Civ. Eng., University of Salerno, Italy.

Sidle, R. C., & Ochiai, H. (2006). Landslides: processes, prediction, and land use (Vol. 18). American Geophysical Union.

Simoni, S., Zanotti, F., Bertoldi, G., & Rigon, R. (2008). Modelling the probability of occurrence of shallow landslides and channelized debris flows using GEOtop- FS. Hydrological Processes, 22(4), 532-545.

Smith, I. M., and D. V. Griffiths (2004),Programming the Finite Element,4th ed., John Wiley, West Sussex, U. K.

Taylor, D. W. (1948), Fundamentals of Soil Mechanics, John Wiley and Sons, N. Y.

Thomas, M. A., Mirus, B. B., Collins, B. D., Lu, N., & Godt, J. W. (2018). Variability in soil-water retention properties and implications for physics-based simulation of landslide early warning criteria. Landslides, 1-13.

Tsai, T. L., & Yang, J. C. (2006). Modeling of rainfall-triggered shallow landslide. Environmental Geology, 50(4), 525-534.

Van Genuchten, M. T. (1980). A closed-form equation for predicting the hydraulic conductivity of unsaturated soils 1. Soil science society of America journal, 44(5), 892-898.

Vingiani, S., Mele, G., Mascellis, R. D., Terribile, F., & Basile, A. (2015). Volcanic soils and landslides: a case study of the island of Ischia (southern Italy) and its relationship with other Campania events. Solid Earth, 6(2), 783-797.

von Bertalanffy, L.: General systems theory: Foundations, Development, Applications, George Braziller Inc., New York, 296 pp.,1968

Wu, W., & Sidle, R. C. (1995). A distributed slope stability model for steep forested basins. Water resources research, 31(8), 2097-2110.

Yeh, H. F., Wang, J., Shen, K. L., & Lee, C. H. (2015). Rainfall characteristics for anisotropic conductivity of unsaturated soil slopes. Environmental Earth Sciences, 73(12), 8669-8681.

Zieher, T., Rutzinger, M., Schneider-Muntau, B., Perzl, F., Leidinger, D., Formayer, H., & Geitner, C. (2017). Sensitivity analysis and calibration of a dynamic physically based slope stability model. Natural Hazards and Earth System Sciences, 17(6), 971.

- Unsaturated soil hydraulic conductivity USHC control rainfall infiltration and slope stability
- We quantified the effect of USHC anisotropy on the hillslope hydrology/stability
- We applied a 3D hydrological model coupled with infinite slope stability model in two test cases
- Results confirm the control of USHC anisotropy on failure time and size of unstable area